Journal of Applied Physics

In situ measurements of the structure and strain of a π-conjugated semiconducting polymer under mechanical load

Cite as: J. Appl. Phys. **127**, 045108 (2020); https://doi.org/10.1063/1.5127226
Submitted: 12 September 2019 . Accepted: 09 January 2020 . Published Online: 29 January 2020

Mouaad Yassine Aliouat, Stéphanie Escoubas, Mohamed Chérif Benoudia, Dmitriy Ksenzov, David Duché, Evangéline Bènevent, Christine Videlot-Ackermann, Jörg Ackermann, Olivier Thomas, and Souren Grigorian

Journal of Applied Physics ARTICLE scitation.org/journal/jap

In situ measurements of the structure and strain of a π-conjugated semiconducting polymer under mechanical load

Cite as: J. Appl. Phys. **127**, 045108 (2020); doi: 10.1063/1.5127226
Submitted: 12 September 2019 · Accepted: 9 January 2020 ·
Published Online: 29 January 2020

Mouaad Yassine Aliouat,[1,2] Stéphanie Escoubas,[1,a)] Mohamed Chérif Benoudia,[2] Dmitriy Ksenzov,[3] David Duché,[2] Evangéline Bènevent,[1] Christine Videlot-Ackermann,[4] Jörg Ackermann,[4] Olivier Thomas,[1] and Souren Grigorian[3,a)]

AFFILIATIONS

[1]Aix Marseille Univ, Université de Toulon, CNRS, IM2NP, Marseille, France
[2]Ecole Nationale Supérieure des Mines et de la Métallurgie, L3M, Annaba, Algeria
[3]Institute of Physics, University of Siegen, D-57068 Siegen, Germany
[4]Aix Marseille Univ, CNRS, CINAM, Marseille, France

[a)]**Authors to whom correspondence should be addressed:** stephanie.escoubas@univ-amu.fr and grigorian@physik.uni-siegen.de

ABSTRACT

In this work, *in situ* studies of organic thin films under stretching are developed. A high efficiency PffBT4T-2OD π-conjugated polymer (PCE11) was coated directly on a stretchable substrate in order to examine the impact of tensile strain on the structural properties. For that purpose, *in situ* grazing incidence x-ray diffraction coupled with optical microscopic observations have been carried out to measure the structural parameters of PCE11 and to probe the mechanical behavior of polymer chains under uniaxial tensile load. It is observed that in the range between 0% and 15%–20% of stretching, the polymer chains become more oriented. Meanwhile, an increase in negative values of deformation, i.e., compression of the polymer chains along the film normal was measured. Beyond this range of stretching, the polymer order declined and the stress was relaxed. This relaxation is explained by the increased number of cracks spreading over the entire film as observed using optical microscopy.

I. INTRODUCTION

The development of polymer-based devices has shown tremendous progress in terms of flexibility and stretchability whether in OLEDs,[1,2] OFETs,[3,4] or OPV.[5–7] It opens extremely promising opportunities and wide research area for innovative and cheap devices.[8] The π-conjugated semiconducting polymers and oligomers are the main elements that compose these devices owing to their optical and semiconductor properties.[9] For photovoltaic applications, the active donor materials must present two basic structural features:[10] First is a π-conjugated backbone composed of a repetition of units resulting in an extended π orbital along the polymer chains, which allows charge transport and optical absorption;[11–13] and second is alkyl side chains that represent the functionalization of the polymer core with solubilizing substituents, which is essential for inexpensive manufacturing by solution methods, as well as to enhance solid state core interactions.[14,15] This renders the polymer soluble in organic solvents such as chlorobenzene (CB), dichlorobenzene, and chloroform.

Moreover, the use of flexible or even stretchable supports, such as poly(dimethylsiloxane) (PDMS),[16] is paving the way to the emergence of the fields of flexible and stretchable electronics and photovoltaic devices,[6,7] which opens many new applications in the fields of entertainment or health thanks to their stretchability[16,17] and biocompatibility,[18,19] and studies such as probing lifetime against mechanical load.[20] Despite the progress in this field, there is still a lack of understanding of the behavior of the structure and optoelectronic properties of the organic materials under mechanical load.

There are only a few reports and studies concerning the mechanical behavior and the change of photovoltaic parameters under mechanical tests.[6,7,21–23] In these studies, stretching and transferring

processes were used to probe the structural and photovoltaic properties and to follow the adhesion of layers using optical microscopy[22] and prestrained PDMS.[6] Only a very little change in photovoltaic properties was reported under high stretching (100% of stretch).[22]

However, the stretching and transferring processes[22] can generate a compression strain during the transfer by stamping. To avoid the impact of layer transferring on the structure, the polymer thin film has been spin-coated directly on the PDMS. Improvement of coating on such stretchable supports will then make it possible to perform *in situ* grazing incidence x-ray diffraction (GIXD) measurements during stretching. GIXD allows probing the structural properties of the crystalline part of the polymer layers. These semicrystalline polymers are weak-scattering materials and their structural features are mainly accessible at the synchrotron radiation sources. Previously, *in situ* GIXD technique was successfully realized for the real-time studies of the formation of the conjugated polymer[24] and oligomer[25,26] films.

In this manuscript, we present a methodology for *in situ* probing of the structural and morphological changes of thin films of poly[(5,6-difluoro-2,1,3-benzothiadiazol-4,7-diyl)-*alt*-(3,3‴-di(2-octyldodecyl)-2,2′,5′,2″,5″,2‴-quaterthiophen-5,5‴-diyl)] (PffBT4T-2OD), called also PCE11, under stretching. PCE11 is one of the most promising donor polymers with high power conversion efficiency in blend with $PC_{71}BM$, and it presents also a relatively good crystallinity.[27–29] Despite mentioned progress, there have been many controversial discussions about the relationship between charge transport and structural order in conjugated polymers,[30,31] and also *in situ* studies to probe the structure and charge mobility upon thermal treatments,[32] to improve efficiency,[33] or to prolong the lifetime.[34] In this work, we studied the structural properties of the donor semicrystalline polymer (PCE11) film, i.e., the changes in the scattered intensity, interplanar distances, and reorientations under tensile strain are measured by *in situ* GIXD using a custom-made stretching device, whereas their morphology is studied employing *in situ* microscopic optical observations of the surface.

II. METHODS

A. Substrates and film preparation

The structure of PCE11 exhibits a π-conjugated backbone and alkyl side chains [the chemical structure is shown in Fig. 1(a)].

The PCE11 powder was purchased from 1-Material Inc., with a purity of 99.99% (major impurities are trace metals), a molecular weight (Mw) of 80 KD, and polydispersity of 2–2.5. The PCE11 was dissolved in CB with a concentration of 15 mg/ml and stirred at 110 °C for more than 1 h into a glovebox with a low oxygen concentration of 200 ppm. The first step in the substrate preparation consists of cleaning and degreasing the surface using acetone, ethanol, and water in an ultrasonic bath during 15 min for each bath, followed by drying using argon flux gas. The surface was activated using UV-ozone treatment for 10 min at 80 °C to improve the wettability on the stretchable substrate.[35,36]

The PCE11 ink was spin-coated both on glass (as a reference) and on the stretchable substrate. We chose PDMS as a stretchable substrate, which is a well suitable support with good mechanical properties (stretching up to 100%) and transparent for photovoltaic (PV) applications. PDMS was obtained by spin-coating with 500 rpm during 11 s using a 184 Silicone Elastomer from Dow Corning on a Kapton support, and then it was annealed at 100 °C during 35 min. The achieved PDMS thickness is 400 μm, measured with a mechanical Bruker Dektak profilometer.

After activation of the substrate surface, we spin-coated the PCE11 ink at 1000 rpm for 1 min on the glass and also directly on the PDMS substrate heated at 110 °C. During the spin-coating, the PDMS substrate was placed on a rigid glass support to improve the homogeneity of the layer.

The size of each PDMS substrate is $36 \times 16\ cm^2$, and the spin-coating was performed in the central area of the PDMS, on a surface of around $16 \times 16\ cm^2$.

We fabricated many samples in order to optimize the PDMS surface treatment and to perform test stretching experiments in the laboratory. Among them, the four most homogeneous were chosen for *in situ* measurements (while stretching) during a synchrotron beamtime.

B. Experimental setup

We performed *in situ* GIXD measurements at beamline BL9 of DELTA synchrotron radiation facility at TU Dortmund, Germany. The photon energy was 15 keV, corresponding to a wavelength of 0.83 Å. We used a wide area image plate 2D MAR3450 detector

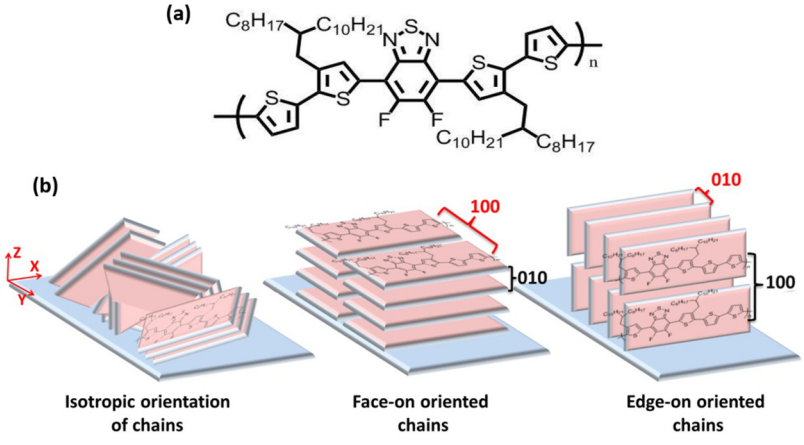

FIG. 1. (a) PCE11 chemical structure and (b) schematic representation of different crystalline packings of π-conjugated polymers.

(3450 × 3450 pixels, with a resolution of 100 μm/pixel). The distance between the sample and the detector was 347 mm, and the calibration was done by measuring the diffraction pattern of a silicon powder. This distance was chosen to be in the range of scattering vector q from 0 to 2 Å^{-1}. A photodiode point detector was used for aligning the sample surface. The incidence angle (α_i) was chosen at 0.1° to be slightly above the critical angle of total reflection of the film and also to be more sensitive to the structure of the whole polymer thin film.

The exposure time was 5 min for each measurement, still avoiding beam damage because the brilliance of this synchrotron is low as compared to other synchrotrons. Indeed, we have tested the beam damage on PCE11 during 1 h exposure time, and we did not see any evolution of the diffraction pattern of the polymer.

In situ GIXD measurements under stretching were carried out by using a specially designed tensile device with controlled load and two moving jaws (where high uniaxial loading can be achieved). The schematic representation of *in situ* stretching GIXD setup is shown in Fig. 2. The x-ray beam was perpendicular to the stretching direction, and after each stretching step, we performed surface alignment to ensure that the measurement was done in the same region during all the experiments.

In situ optical microscopic observations were performed during stretching to probe the microstructure of the layers by using an OLYMPUS DP71 optical microscope with a magnification of 11.5. This optical microscope was fixed on the stretching machine in a way to observe the same area on the sample surface.

III. RESULTS AND DISCUSSION

A. Polymer film orientations

The structure of π-conjugated semiconducting polymers is semicrystalline with polymer chain orientation either isotropic or exhibiting a preferential orientation like edge-on or face-on [Fig. 1(b)]. In face-on orientation, the interchain distance is parallel to the substrate surface, whereas in edge-on orientation this distance is perpendicular to the surface.

GIXD measurements allow determining the orientation and the different distances between polymer chains. These distances correspond either to a lamellar stacking that gives rise to h00 peaks or to the aromatic π–π stacking that gives rise to 0k0 peaks. Through red and black colors in Fig. 1(b), we schematically indicate the interplanar distance that contributes to diffraction peaks along the in-plane and out-of-plane directions, respectively.

B. From rigid to stretchable substrate

The 2D GIXD patterns of PCE11 spin-coated on glass and on PDMS substrates are represented in Figs. 3(a) and 3(b), respectively. Both patterns show the strongest scattered intensity along the vertical (q_z) axis, which corresponds to the out-of-plane direction. The pattern in Fig. 3(a) reveals a highly edge-on oriented PCE11 film coated on glass, with the strongest h00 peak being detectable until the fourth order along the out-of-plane direction (q_z). The aromatic π–π stacking ring along both the out-of-plane (q_z) and the in-plane (q_x) directions are also visible (010 peak). On the other hand, the pattern of PCE11 coated on PDMS [Fig. 3(b)] reveals a less edge-on oriented film, with the 100 peak only visible until the second order along q_z and a weak peak along (q_x), together with a pronounced contribution of the amorphous PDMS ring.

In order to quantify the orientation of polymer chains and to probe the anisotropy, we performed an azimuthal integration of the patterns by an arc-cut to the 100 peak, characterized by its radius, width, center, and its angular range [see Fig. S1(a) in the supplementary material]. These parameters were chosen in order to integrate all the scattered intensities of the peak. The intensities of the 100 lamellar peak, as a function of the angular range $-85° < \chi < 85°$, are shown in Figs. 3(c) and 3(d). This range was selected because of the weak signal for $|\chi| > 85°$ probably caused by the surface roughness of samples.

As shown schematically in Fig. 1(b), we can distinguish three orientations: edge-on, face-on, and isotropic. If the scattered intensity arises from the edge-on oriented chains, we can include all chains with an orientation close to $\chi = 0°$, and the intensity at $\chi = 85°$ or $-85°$ indicates the face-on oriented chains. In the isotropic case, the scattering intensity arising from the subset of chains forms a uniform ring with a random distribution.[37]

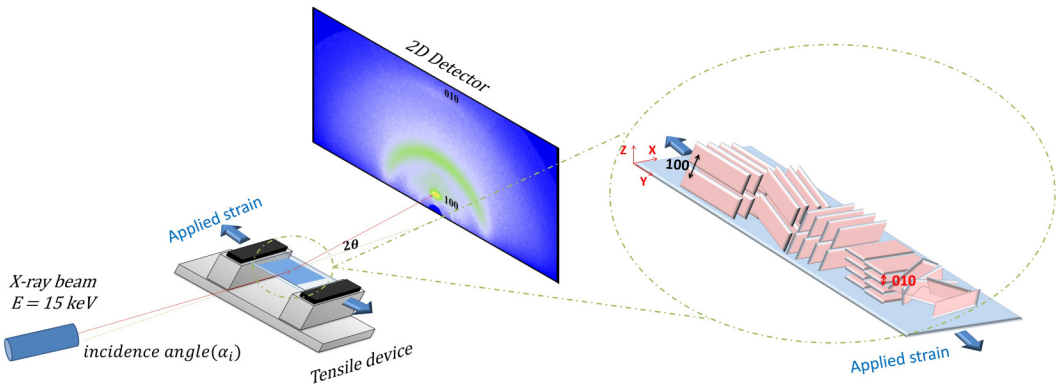

FIG. 2. Schematic view of *in situ* stretching GIXD experimental setup.

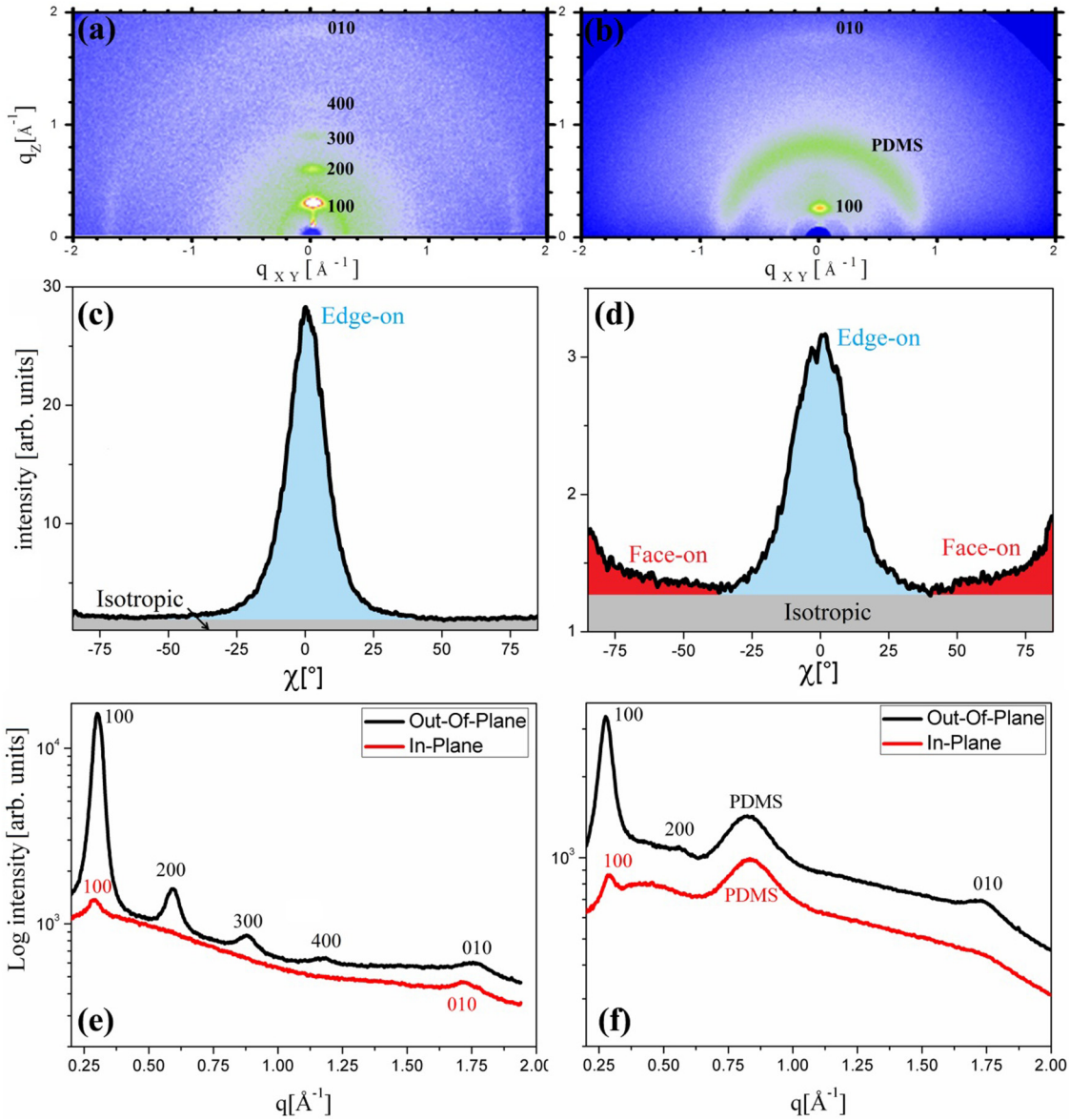

FIG. 3. 2D GIXD pattern of PCE11 spin-coated on (a) glass and (b) PDMS. The azimuthal integration along χ shows the anisotropy of the chain orientation and the portions of face-on or edge-on orientations for the 100 peak of PCE11 spin-coated on (c) glass and (d) PDMS. The corresponding out-of-plane and in-plane integrations show the different peaks of PCE-11 spin coated on (e) glass and (f) PDMS.

For the film coated on a glass substrate [Fig. 3(c)], most of crystalline polymer chains are edge-on oriented (~80%), and the remaining fraction is isotropic. For the layers coated on PDMS [Fig. 3(d)], the crystalline regions are mostly edge-on oriented or isotropic with portions of ~46% or ~45%, respectively, but there is also a small portion that is face-on oriented. From comparison of these two cases, it follows that the films spin-coated on glass are mostly edge-on oriented and more ordered than on PDMS with an FWHM in χ being 1.4 times broader. These results mean that the preferential orientation and the ordering of polymer chains are substrate-dependent.

Using the integration of pie-cuts along q_z and q_x directions [see Fig. S1(a) in the supplementary material], we extracted the curves of scattering intensity in the out-of-plane and in-plane directions, as shown in Figs. 3(e) and 3(f) for both samples.

Along q_z, we measured the distance between the edge-on oriented polymer chains giving rise to the lamellar peak 100, and

TABLE I. Main structural parameters: peak center, polymer chains spacing (Å), FWHM ($Å^{-1}$), and integrated intensity of the lamellar peak along q_z and q_x directions of PCE11 spin-coated on glass and PDMS substrates [from Figs. 3(e) and 3(f)].

	Glass substrate		PDMS substrate	
100 lamellar peak	OOP (q_z)	IP (q_x)	OOP (q_z)	IP (q_x)
Measured integrated intensity (a.u.)	636	16.2	17.5	7.0
Measured peak position ($Å^{-1}$)	0.30	0.29	0.28	0.29
Calculated spacing (Å)	20.8	21.7	22.8	21.7
Measured FWHM ($Å^{-1}$)	0.043	/	0.057	/
Calculated coherence length L_c (Å) with Scherrer formula (1)	131	/	101	/

also the aromatic π–π stacking spacing (010 weak peak) of the face-on oriented chains that are perpendicular to the substrate.

Along q_x we may extract the distance between the face-on oriented polymer chains giving rise to a weak lamellar peak, and the π–π stacking spacing of the edge-on oriented chains that are parallel to the substrate.

For the 100 lamellar peak along out-of-plane (OOP) q_z and in-plane (IP) q_x directions, we extracted the integrated intensity, the peak center, and the FWHM of each sample. The results are shown in Table I.

In Table I, by comparing the measured integrated intensities along q_z and q_x directions, we can see clearly that the layers are strongly edge-on ordered both on glass and on the PDMS substrate. However, we obtained a ratio of integrated intensities between both directions [ratio = Integrated intensity (q_z)/Integrated intensity (q_x)] of 40 for the PCE11 layer coated on glass and only 18 for PCE11 on PDMS, confirming that the polymer chains of the PCE11 layer coated on the glass substrate show dominating edge-on orientation in comparison to the PDMS substrate. Thus, the intensity of 100 peak of PCE11 on glass is around 7 times higher than the one obtained on PDMS, and the FWHM is about 30% smaller. From the FWHM Δq of each peak, the size of coherent domains can be calculated by the following Scherrer formula:

$$L_C = 2\pi \frac{0.9}{\Delta q}. \quad (1)$$

Assuming homogeneous distribution of d-spacings, the value obtained on glass is 1.3 times larger than on PDMS. The difference on FWHM could also be attributed to microstrains (distribution of d-spacings) or disorder that is probably more important on PDMS.

Peak broadening has multiple causes that in common cases can be separated into two main contributions: (i) crystallite size broadening that is independent of the Bragg peak position, and (ii) lattice disorder broadening that depends on the Bragg peak position. Both contributions can be well estimated for the PCE11 layer coated on the glass substrate, with more than two Bragg reflections to decouple these parameters. Considering the distribution of lattice spacing in q space as a function of lattice parameter d, one could obtain[38]

$$\frac{\Delta q^2}{(2\pi)^2} = \left(\frac{0.9}{L_a}\right)^2 + \frac{(\pi g)^4}{d^2}\, n^4, \quad (2)$$

where L_a is the crystallite size and g is the paracrystalline disorder parameter.

Dependence of Δq^2 as a function of n^4, for three orders of n of the h00 Bragg peak, reveals a g-factor equal to 4.5% (Table II), with a crystallite size of 119 Å.

Thus, introducing this disorder parameter is more realistic, and the calculated size of coherent domains L_c is even smaller than without this g parameter.

The extraction of physical parameters from the Bragg peak width is more difficult for PCE11 coated on PDMS, since only one diffraction order is really measurable, which does not allow such a decoupling to be done. In this case, two boundary assumptions can be done:

(1) Disorder is supposed to be the same as for the films deposited on glass ($g = 4.5\%$ like on the glass substrate); we obtain an estimated size of crystalline domains $L_a = 99$ Å.

TABLE II. Comparison of crystallite size and disorder parameter of PCE11 layers coated on glass and on PDMS substrate.

100 lamellar peak	Glass substrate	PDMS substrate
Measured FWHM ($Å^{-1}$)	0.043	0.057
First order Bragg peak		
Calculated crystallite size L_c (Å) with Scherrer formula (1)	131	101
Calculated disorder parameter g (%)	4.5	…
Calculated crystallite size L_a (Å) assuming disorder parameter	119	…
Estimated disorder parameter g (%) with fixed crystallite size L_a	…	10.7
Estimated crystallite size L_a (Å)	…	99
with fixed disorder parameter g		

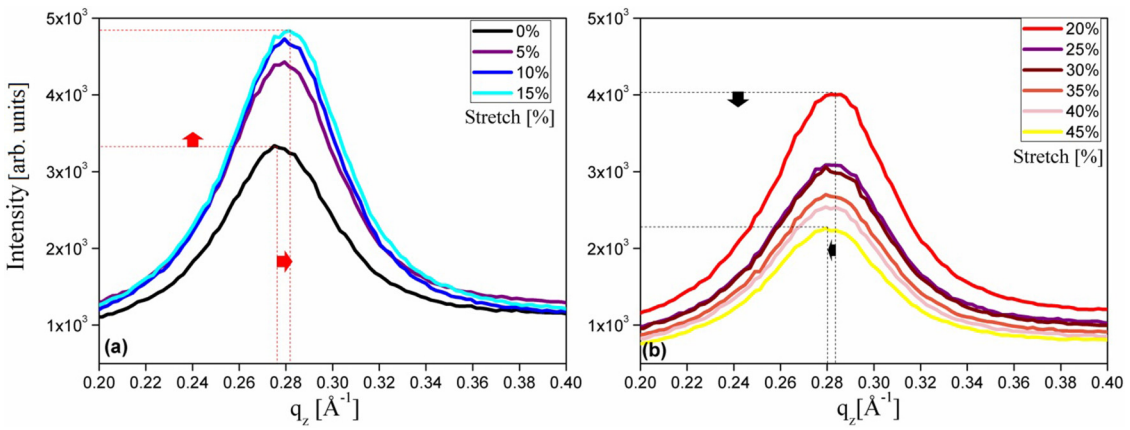

FIG. 4. The out-of-plane integration showing the evolution of the 100 lamellar peak (a) under [0%:15%] of stretching and (b) under [20%:45%] of stretching.

(2) Coherent domain size is supposed to be the same as on the glass substrate ($L_a = 119$ Å), which gives an estimated value of disorder of $g = 10.7\%$.

In any case, these differences between the two substrates mean that the layers coated on glass are more ordered and better crystallized than on PDMS.

C. Structural properties evolution under mechanical load

In situ GIXD measurements were performed under uniaxial tensile test to probe the impact of stress on the molecular ordering of the polymer chains and their deformation. We plotted the intensity evolution of the out-of-plane lamellar 100 peak vs the scattering vector q_z ($Å^{-1}$) for different values of stretching (the stretch is calculated via the relative distance between the tensile device jaws). These curves are extracted from the pie-cut integration of recorded 2D images as explained in Sec. III A.

From the curves of Fig. 4, we can see two different trends. First [Fig. 4(a)], from 0% to 15% of stretching, a shift of the peak position to higher q_z values is evidenced, which means that the vertical spacing between polymer chains decreases under stretching. Second [Fig. 4(b)], after reaching a critical value between 15% and 20% of stretching, an opposite shift of the peak position to smaller values of q_z is observed, corresponding to an increasing spacing.

Figure 5(a) shows the changes in integrated intensity ΔI as a function of applied stretch for the out-of-plane 100 peak,

$$\Delta I(\%) = 100(I - I_0)/I_0. \quad (3)$$

Until 15% of stretching, a remarkable increase in the integrated intensity by 76% is evidenced, meaning that the amount of edge-on ordered polymer chains increases until this value of stretching.

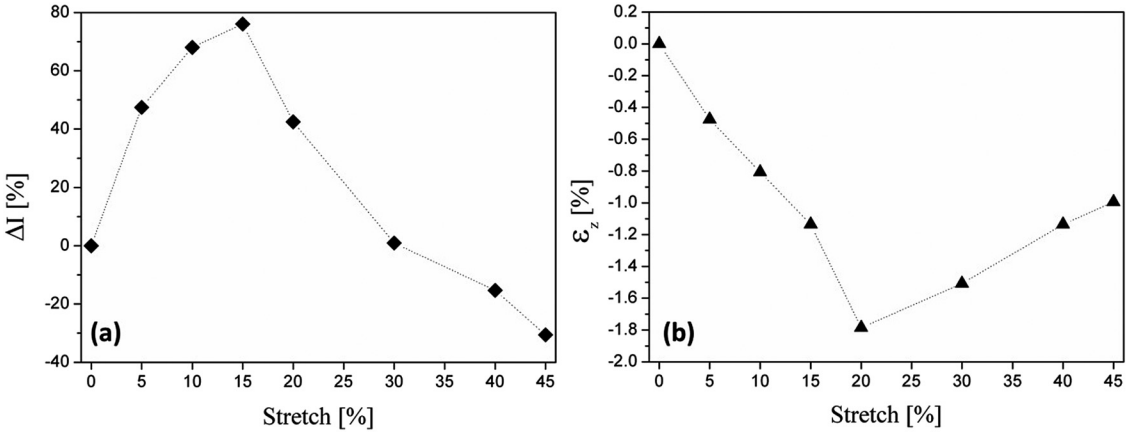

FIG. 5. (a) The change in normalized integrated intensity of the 100 lamellar peak vs stretching. (b) The strain evolution of the 100 lamellar spacing under stretching.

We calculated the evolution of the edge-on area ratio during stretching and we obtained an increase of 65% (at 15% stretch). For larger deformations, the integrated intensity decreases steadily, reaching a value similar to the initial state at 30% of stretching and going to lower values for even larger deformations, which corresponds to a decrease of edge-on oriented chains in the crystalline regions.

In order to better quantify the mechanical behavior of the layers, we calculated the strain (ε) of polymer chains along q_z, which is defined as the change of the spacing between polymer chains ($d - d_0$) divided by the initial spacing (d_0),

$$\varepsilon_z = 100(d - d_0)/d_0. \quad (4)$$

Figure 5(b) shows the strain evolution of polymer chains along q_z. The negative values of ε_z can be interpreted as a Poisson compressive strain resulting from the applied stress along the Y stretching direction. Assuming perfect adhesion, the strain of the film along Z should be

$$\varepsilon_{33f} = -\nu_f \frac{1 - \nu_s}{1 - \nu_f} \varepsilon_{11S}, \quad (5)$$

where ν_s and ν_f are, respectively, the Poisson ratios of the substrate and film and ε_{11S} is the applied strain on the substrate. Poisson ratio of PDMS is 0.5,[21] and we assume a Poisson ratio of 0.35 for PCE11 (as for P3HT).[37]

The strain along Z should be −5.4% at 20% of stretching. However, for the 100 lamellar peak, until 20% of stretching, the deformation value for PCE11 goes down from 0% to −1.78%, roughly linearly. Above 20% stretching, we observe stress relaxation (back to −0.99% of deformation when the substrate is broken). Since the maximum observed strain is −1.8% instead of the predicted −5.4%, one has to assume a reduced load transfer from the substrate to the crystalline regions of the polymer; this could be explained by the fact that the applied strain is mostly distributed in the amorphous regions of the polymer. For the aromatic π–π stacking peak (not shown here) along the vertical direction, the polymer chains are also under negative strain, but after 20% of stretching it becomes more difficult to determine the strain evolution because the diffraction peak is very weak. Comparing the strain of the polymer chains between these two orientations, we measured −1.78% and −0.4% of strain for the lamella (edge-on) and the π–π stacking (face-on), respectively, under 20% of stretching, which shows the anisotropic character of elasticity in the polymer. This may explain the anisotropic properties of the layer and the good photovoltaic and electrical properties of these polymers under mechanical load as well.[21] Furthermore, charge transport is highly anisotropic in π-conjugated systems, being most effective along the aromatic π–π stacking direction giving rise to 010 peak and poor along the insulating alkyl side chains between the lamellar distances giving rise to 100 lamellar peak.[39–41]

D. *In situ* optical microscope observations of the surface

To follow the microstructure and get insights into the origin of the relaxation mechanism that works above 20% stretching, we also performed *in situ* microscopic observations of the PCE11 surface under stretching. The images under stretching are shown in Fig. 6 and demonstrate cracking of the polymer surface. The crack-onset strain is of the order of 10%, and cracking dominates the mechanical behavior beyond 18%–20%. Lipomi *et al.* also observed the first cracking of layers between 8% and 12% and the cracks spreading at 20% of stretching.[6]

For a better quantification of these images, statistics on the cracks were performed to extract their dimensions (width and length) and their number. For that purpose, we considered elliptic shapes, and we took into account only defects bigger than 100 μm^2 on a surface unit of 1 cm^2. For the crack dimension estimation, the average value of length and width was taken into account, with a standard deviation of about 20 μm because the crack's sizes are not homogeneous. The total area was calculated by taking the sum of all crack areas. The *in situ* evolution of the number and dimensions of cracks and their normalized total area are shown in Fig. 7.

As shown in Fig. 7(a), the number of cracks increases dramatically in the range from 15% to 25% of stretching (15 times at 20%). The length of cracks increases faster than the width, and the

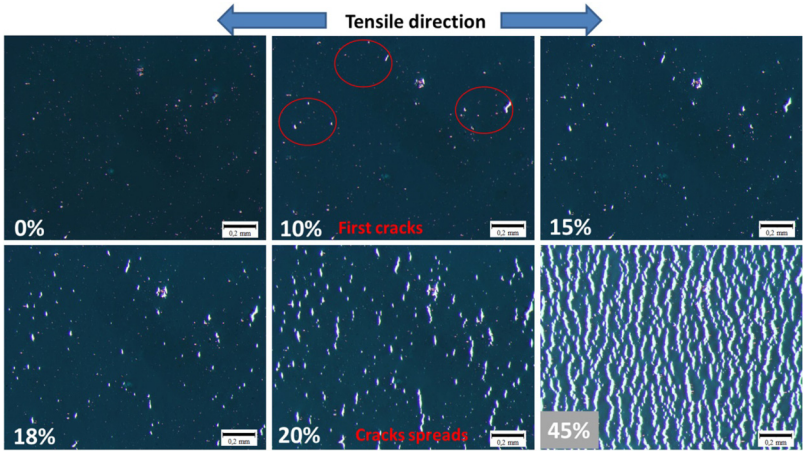

FIG. 6. Optical microscope images of the surface of the PCE11 layer under stretching.

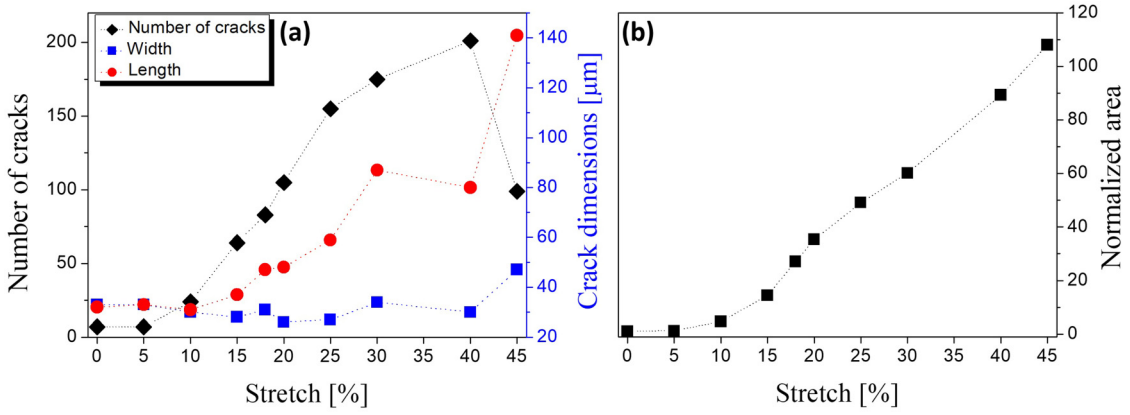

FIG. 7. The evolution of (a) the average width, the average length, and the number of cracks; and (b) the normalized total area of cracks, under stretching.

propagation of cracks is almost perpendicular to the stretching direction. The decrease in the number of cracks between 40% and 45% of stretching is explained by the fact that the cracks coalesce. Besides, the total area is always increasing under stretching [Fig. 7(b)].

Overall, the *in situ* optical microscope observations are in good correlation with the GIXD measurements. These observations show that after a critical value of 10%–15% stretching, cracking occurs in the polymer layer. At the same time, the average elastic strain measured by GIXD decreases as a consequence of stress relaxation along the crack boundaries. The elastic strain energy stored in the PCE11 films decreases as a result of increasing crack length developed upon stretching higher than 20%.

Moreover, recycle experiments have been performed on blend polymer films (in the range 0%–10% of stretch), and in this range, we could observe a reversible behavior. We may assume from cycling experiments that there is a reversible regime at least up to 10% stretch.

IV. CONCLUSION

We studied the structure of the PCE11 π-conjugated polymer layer under mechanical load on a stretchable support by using *in situ* GIXD measurements coupled with optical observations. This study reveals that spin-coated layers of this polymer are mostly edge-on oriented. Tensile tests show that in the out-of-plane direction the polymer chains which are perpendicular to the stretching direction undergo increasing compressive strain until 15%–20% stretching in agreement with a Poisson effect. Further on, beyond 20%, a partial strain relaxation takes place. Optical observations indicate that massive crack propagation occurs at 20% of stretching, which explains the strain relaxation. Comparing the imposed displacement with the measured strain, a weak load transfer from the substrate to the crystalline part of the polymer is inferred, which leads to the conclusion that the applied tension may be distributed in the amorphous regions of the polymer that plays a role of a force damper. The polymer chains are less sensitive to the applied tension along the aromatic π–π stacking order. This behavior has to be confirmed on blends and is correlated with the good photovoltaic properties of layers before cracking spreads at 20% stretching.[22] Beyond the results specific to PCE11 films, the presented *in situ* method can be applied to any partially crystallized polymer films for stretchable electronics. This setup allows for a very detailed *in situ* investigation of the structure under stretching in these polymer films or blends.

SUPPLEMENTARY MATERIAL

See the supplementary material for a description of intensity integration of 2D GIXD pattern, in order to obtain line profiles in Fig. 3.

ACKNOWLEDGMENTS

This work was supported by DAAD-PROCOPE (Project No. 57211900, Campus France 35484SE) and PHC-Tassili (Project No. 17MDU994). We are grateful to S. Laifa for assistance in PDMS supports elaboration; L. Grodd, K. Shchyrba, and the mechanical workshop at the University of Siegen for assistance in the construction of the stretching device; and C. Sternemann and M. Paulus for support during the experiment at BL9 beamline at the DELTA synchrotron (Dortmund, Germany).

REFERENCES

[1] A. Sugimoto, H. Ochi, S. Fujimura, A. Yoshida, T. Miyadera, and M. Tsuchida, IEEE J. Sel. Top. Quantum Electron. **10**, 107 (2004).
[2] M.-C. Choi, Y. Kim, and C.-S. Ha, Prog. Polym. Sci. **33**, 581–630 (2008).
[3] T. Sun, J. I. Scott, M. Wang, R. J. Kline, G. C. Bazan, and B. T. O'Connor, Adv. Electron. Mater. **3**, 1600388 (2017).
[4] B. H. Lee, B. B. Y. Hsu, S. N. Patel, J. Labram, C. Luo, G. C. Bazan, and A. J. Heeger. Nano Lett. **16**, 314–319 (2016).
[5] Z. Liu, J. Li, and F. Yan, Adv. Mater. **25**, 4296–4301 (2013).
[6] D. J. Lipomi, B. C.-K. Tee, M. Vosgueritchian, and Z. Bao, Adv. Mater. **23**, 1771–1775 (2011).
[7] S. J. Benight, C. Wang, J. B. H. Tok, and Z. Bao, Prog. Polym. Sci. **38**, 1961–1977 (2013).
[8] B. C. Thompson and J. M. J. Fréchet, Angew. Chem. Int. Ed. **47**(1), 58–71 (2008).

[9]A. Facchett, Chem. Mater. **23**, 733–758 (2011).
[10]N. Karl, Synth. Met. **133–134**, 649–657 (2003).
[11]H. Sirringhaus, Nat. Mater. **2**, 641 (2003).
[12]A. Pron and P. Rannou, Prog. Polym. Sci. **27**, 135 (2002).
[13]F. Cacialli, Philos. Trans. R Soc. Lond. Ser. A. **358**, 173 (2000).
[14]H. E. Katz, Chem. Mater. **16**, 4748 (2004).
[15]S. Allard, M. Forster, B. Souharce, H. Thiem, and U. Scherf, Angew. Chem. Int. Ed. **47**, 4070 (2008).
[16]M. C. LeMieux and Z. Bao, Nat. Nanotechnol. **3**, 585 (2008).
[17]J. A. Rogers, T. Someya, and Y. G. Huang, Science **327**, 1603 (2010).
[18]T. Someya, Nat. Mater. **9**, 879 (2010).
[19]R. H. Kim, D. H. Kim, J. L. Xiao, B. H. Kim, S. I. Park, B. Panilaitis, R. Ghaffari, J. M. Yao, M. Li, Z. J. Liu, V. Malyarchuk, D. G. Kim, A. P. Le, R. G. Nuzzo, D. L. Kaplan, F. G. Omenetto, Y. G. Huang, Z. Kang, and J. A. Rogers, Nat. Mater. **9**, 929 (2010).
[20]F. C. Krebs, T. D. Nielsen, J. Fyenbo, M. Wadstrøm, and M. S. Pedersen, Energy Environ. Sci. **3**, 512 (2010).
[21]D. J. Lipomi, H. Chong, M. Vosgueritchian, J. Mei, and Z. Bao, Sol. Energy Mater. Sol. Cells **107**, 355–365 (2012).
[22]C. Lu, W.-Y. Lee, X. Gu, J. Xu, H.-H. Chou, H. Yan, Y.-C. Chiu, M. He, J. R. Matthews, W. Niu, J. B.-H. Tok, M. F. Toney, W.-C. Chen, and Z. Bao, Adv. Electron. Mater. **3**, 1600311 (2017).
[23]B. O'Connor, R. J. Kline, B. R. Conrad, L. J. Richter, D. Gundlach, M. F. Toney, and D. M. DeLongchamp, Adv. Funct. Mater. **21**, 3697–3705 (2011).
[24]L. Grodd, U. Pietsch, and S. Grigorian, Macromol. Rapid Commun. **33**, 1765–1769 (2012).
[25]E. Mikayelyan, A. V. Bakirov, M. A. Shcherbina, S. N. Chvalun, S. A. Ponomarenko, and S. Grigorian, RSC Adv. **5**, 1319–1322 (2015).
[26]S. Grigorian, S. Escoubas, D. Ksenzov, D. Duche, M. Aliouat, J.-J. Simon, B. Bat-Erdene, S. Allard, U. Scherf, U. Pietsch, and O. Thomas, J. Phys. Chem. C **121**(41), 23149–23157 (2017).
[27]J. Zhao, S. Zhao, Z. Xu, B. Qiao, D. Huang, L. Zhao, Y. Li, Y. Zhu, and P. Wang, ACS Appl. Mater. Interfaces. **8**, 18231–18237 (2016).
[28]Q. Sun, F. Zhang, Q. An, M. Zhang, J. Wang, and J. Zhang, Phys. Chem. Chem. Phys. **19**, 709 (2017).
[29]H. W. Ro, J. M. Downing, S. Engmann, A. A. Herzing, D. M. DeLongchamp, L. J. Richter, S. Mukherjee, H. Ade, M. Abdelsamie, L. K. Jagadamma, A. Amassian, Y. Liu, and H. Yan, Energy Environ. Sci. **9**, 2835 (2016).
[30]R. Noriega, J. Rivnay, K. Vandewal, F. P. V. Koch, N. Stingelin, P. Smith, M. F. Toney, and A. Salleo, Nat. Mater. **12**, 1038–1044 (2013).
[31]T. Heumueller, W. R. Mateker, A. Distler, U. F. Fritze, R. Cheacharoen, W. H. Nguyen, M. Biele, M. Salvador, M. von Delius, H.-J. Egelhaaf, M. D. McGehee, and C. J. Brabec, Energy Environ. Sci. **9**, 247–256 (2016).
[32]S. Joshi, P. Pingel, S. Grigorian, T. Panzner, U. Pietsch, D. Neher, M. Forster, and U. Scherf, Macromolecules **42**, 4651 (2009).
[33]G. Li, R. Zhu, and Y. Yang, "Polymer solar cells," Nat. Photonics **6**, 153–161 (2012).
[34]M. Jørgensen, K. Norrman, and F. C. Krebs, Sol. Energy Mater. Sol. Cells **92**, 686 (2008).
[35]K. Efimenko, W. E. Wallace, and J. Genzer, J. Colloid Interface Sci. **254**, 306–315 (2002).
[36]C. M. Stafford, C. Harrison, K. L. Beers, A. Karim, E. J. Amis, M. R. Vanlandingham, H. C. Kim, W. Volksen, R. D. Miller, and E. E. Simonyi, Nat. Mater. **3**, 545 (2004).
[37]S. E. Root, S. Savagatrup, C. J. Pais, G. Arya, and D. J. Lipomi, Macromolecules **49**(7), 2886–2894 (2016).
[38]T. G. Dane, J. E. Bartenstein, B. Sironi, B. M. Mills, O. A. Bell, J. E. Macdonald, T. Arnold, C. F. J. Faul, and W. H. Briscoe, Phys. Chem. Chem. Phys. **18**, 24498–24505 (2016).
[39]A. Hamidi-Sakr, L. Biniek, S. Fall, and M. Brinkmann, Adv. Funct. Mater. **26**, 408–420 (2016).
[40]E. J. W. Crossland, K. Tremel, F. Fischer, K. Rahimi, G. Reiter, U. Steiner, and S. Ludwigs, Adv. Mater. **24**, 839 (2012).
[41]L. H. Jimison, M. F. Toney, I. McCulloch, M. Heeney, and A. Salleo, Adv. Mater. **21**, 1568 (2009).